IDETC/CIE 2015-47139

A NETWORK OF TYPE III BRICARD LINKAGES

Shengnan Lu
PMAR Robotics, University of Genoa
Genoa, Italy 16145
Robotics Institute, Beihang University
Beijing, China 100191
Email: lvshengnan5@gmail.com

Dimiter Zlatanov
PMAR Robotics
University of Genoa
Genoa, Italy 16145
Email: zlatanov@dimec.unige.it

Xilun Ding
Robotics Institute
Beihang University
Beijing, China 100191
Email: xlding@buaa.edu.cn

Matteo Zoppi
PMAR Robotics
University of Genoa
Genoa, Italy 16145
Email: Zoppi@dimec.unige.it

Simon D. Guest
Department of Engineering
University of Cambridge
Cambridge CB2 1PZ, UK
Email: sdg@eng.cam.ac.uk

ABSTRACT

*Among Bricard's overconstrained 6R linkages, the third type
has two collapsed configurations, where all joint axes are copla-
nar. The paper presents a one-degree-of-freedom network of
such linkages. Using the two coplanar states of the constituent
Bricard units, the network is able to cover a large surface with a
specific outline when deployed, and can be folded compactly into
a stack of much smaller planar shapes. Five geometric parame-
ters describing each type III Bricard mechanism are introduced.
Their influence on the outline of one collapsed configuration is
discussed and inverse calculation to obtain the parameter values
yielding a desired planar shape is performed. The network is
built by linking the units, either using scissor linkage elements, if
the thickness of the panels can be ignored, or with hinged paral-
lelograms, for a thicker material. Two case studies, in which the
Bricard network deploys as a rectangle and a regular hexagon,
respectively, are presented, validating the analysis and design
methods.*

INTRODUCTION

Deployable mechanisms (DMs), which are capable of large
change in their physical size, have many potential applications in
areas such as temporary and emergency architecture and space
structures, including antennas and telescopes [1–3]. The scissor
linkage has been used as a simple basic element in many creative
designs of deployable mechanisms, as in the famous Hoberman
polyhedral mechanism [4]. Maden has systematically analyzed
the behavior of the scissor linkage as a basic unit of deployable
mechanisms with different expansion patterns [5]. Recently, in
search of good stiffness and high expansion to package ratio,
more attention has been paid to spatial over-constrained linkages
as possible building units for the design of deployable mecha-
nisms. Chen et al. have proposed several mobile assemblies
which are composed of the Bennett linkages, the Myard linkages,
or the Bricard linkages [6, 7]. Qi et al. have built a prototype of
DM based on the Myard linkages [8].

The type III Bricard linkage, which has two collapsed con-
figurations (i.e., states where all the revolute joints are copla-
nar), has attracted less attention compared to other Bricard type-
s [9–11]. Due to the ability to collapse in two ways, a network

1

of type III linkages can cover a large surface with a specific outline when deployed, and can be folded compactly into a stack of much smaller planar shapes. In this study, we discuss how to build and shape such a network by linking Bricard linkages with either the same or different geometric parameters.

The paper is organized as follows. In the following section, the type III Bricard linkage is reviewed and parameterized. Then, the two collapsed configurations of the mechanism are analyzed, including the influence of the parameters on the planar shape. Next, the range constraints of the parameters are discussed. Inverse calculation of obtaining the parameter values of a specific deployed configuration is derived. Then, two methods of connecting linkages are proposed to build the network. Two case studies are performed to obtain different deployed shapes, and each is validated by a simulation.

TYPE III BRICARD LINKAGE
Geometric Construction

The Bricard linkage $ABCA'B'C'$ in Fig. 1, is of type III with two collapsed states. The linkage can be constructed as follows: draw two concentric circles of arbitrary radii; choose two arbitrary points A and A' outside of the larger circle; construct the tangents from A and A' to the circles and determine their intersections B, B', C and C'. The lines BC, $B'C'$, $B'C$ and BC' will be tangent to a third concentric circle with radius r_t. Then the six triangles ABC', ABC, $A'BC$, $A'B'C$, $A'B'C'$, $AB'C'$ taken in that cyclic order, hinged at their common edges, constitute a deformable six-plate linkage with 1 dof [12].
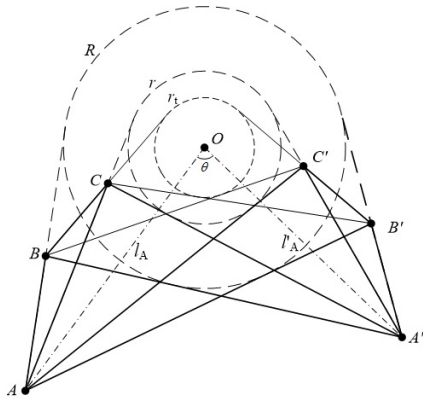

FIGURE 1.   Construction of a Bricard linkage

The six triangles in fact define a deformable octahedron: the two remaining (virtual) faces are the triangles ACB' and $A'C'B$, whose shape is constant during the movement. However, if they are physically part of the linkage, link interference is unavoid-

able. Furthermore, any six of the eight faces can be hinged together, generating an equivalent motion of the octahedron.

Parametrization of the Bricard linkage

The construction in Fig. 1, can be described by the radii of the two circles and the positions of points A and A'. We denote the radii of the larger and smaller concentric circles by R and r, respectively. The lengths of OA and OA' are l_A and l'_A. The fifth parameter, is the angle between OA and OA', denoted by θ. A Bricard linkage will be decided by those five scalars, R, r, l_A, l'_A, and θ. One of the five parameters controls the scale of the Bricard linkage; the other four decide the collapsed configuration, which determines the shape and movement of the Bricard linkage.

GEOMETRY ANALYSIS OF TYPE III BRICARD LINKAGE

In this study, the two collapsed configurations of the Bricard linkage will be the compact and deployed configuration in the network. The hexagon in Fig. 1 is the compact configuration of the Bricard linkage and also the network. The deployed configuration determines the outline of the deployed network. Limitations of the 5 parameters are analyzed; their influence on the outline of the deployed configuration is discussed. Back calculations are performed in the end of this section.

The two collapsed configurations

Figure 1 shows one of the collapsed configurations of the type III Bricard linkage. It also reveals the relationships among the rotation axes in this configuration. Linking the 6 axes, AB, BC, CA', $A'B'$, $B'C'$, $C'A$ in a circle, an overconstrained mechanism with 1 dof is constructed, Fig. 2. And the mechanism can move from one collapsed configuration to the other one.
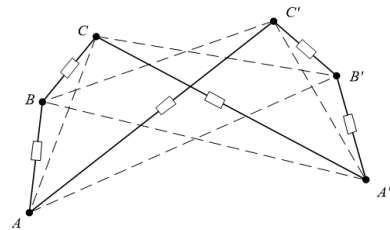

FIGURE 2.   Schematic of the type III Bricard linkage

Each pair of adjacent axes intersect, which indicates the length of each link (the common normal of the two adjacent axes) is 0. However, the distance between each two adjacent vertices

remains constant. In the following, we focus on the geometric shape (outline) of the polygon configured by the 6 vertices. An example of these two configurations of a Bricard linkage is shown in Fig. 3.
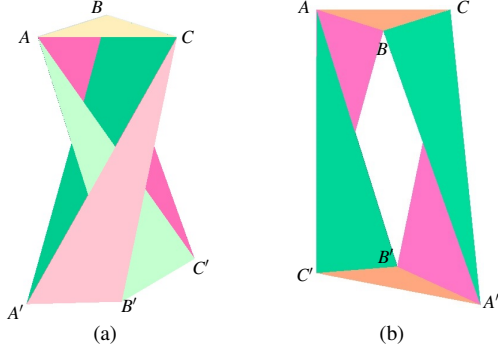

FIGURE 3. Two collapsed configurations of the type III Bricard

In Fig. 3(a), the polygon is a hexagon, described by the location of all the 6 vertices. It is a quadrangle in Fig. 3(b), which is determined only by vertices, A, C, A', C'.

If we see the quadrangle as a four-bar mechanism with known link lengths, at least an angle is required to decide its configuration, which means that in total 5 parameters can determine a quadrangle (there will be two solutions with the given 5 parameters, however, herein only the unique convex quadrangle is considered). As a type III Bricard linkage is also described by 5 parameters, there will be a one-to-one mapping between the Bricard linkage and the formed quadrangle. (This conclusion is also consistent with the dof of the mechanism being 1.)

The relationship of the shape of the quadrangle $ACA'C'$ and the 5 parameters of the Bricard linkage are calculated in the following.

The angles are named as follows, $\angle OAB = \alpha_{A1}$, $\angle OAC = \alpha_{A2}$, $\angle BAB' = \beta_A$, $\angle BA'B' = \beta_A'$.

As AB and AB' are tangent to the big circle, Fig. 1,

$$\angle OAB = \angle OAB' \qquad (1)$$

$$\beta_A = 2\alpha_{A1} = 2\arcsin\frac{R}{l_A}. \qquad (2)$$

As AC and AC' are tangent with the small circle,

$$\angle OAC = \angle OAC' \qquad (3)$$

Therefore,

$$\angle BAC = \angle B'AC'. \qquad (4)$$

In Fig. 3(a), it can be seen that $\angle BAB' = \angle B'AC' + \angle BAC'$. Similarly, from Fig. 3(b), $\angle CAC' = \angle BAC + \angle BAC'$. From (4),

$$\angle CAC' = \beta_A = 2\arcsin\frac{R}{l_A} \qquad (5)$$

where $\angle CAC'$ is in the deployed configuration.

As a flexible octahedron, the six triangles remain congruent in both collapsed configurations, and throughout the motion.

Similarly,

$$\angle CA'C' = \beta_A' = 2\arcsin\frac{R}{l_A'}. \qquad (6)$$

Because of symmetry, it is sufficient to consider the case $l_A \geqslant l_A'$, which implies $\beta_A \leqslant \beta_A'$.

The edges of the quadrangle are AC, $A'C$, AC', $A'C'$. They are the tangent lines from A and A' to the small circle, Fig. 4.
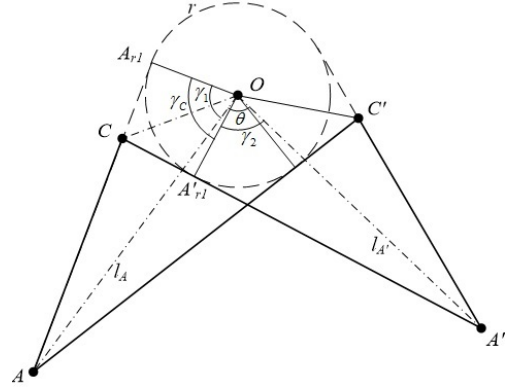

FIGURE 4. Dimensions of the quadrangle

Herein,

$$\gamma_1 = \arcsin\frac{r}{l_A} \qquad (7)$$

$$\gamma_2 = \arcsin\frac{r}{l_A'} \qquad (8)$$

3

$$\gamma_c = \gamma_1 - \gamma_2 + \theta \tag{9}$$

A_{r1} and A'_{r1} are the points of tangency from A and A' to the small circle. So,

$$|AA_{r1}| = \sqrt{l_A^2 - r^2} \tag{10}$$

$$|CA_{r1}| = r\tan\frac{r_c}{2} = r\tan\frac{\arcsin\frac{r}{l_A} - \arcsin\frac{r}{l'_A} + \theta}{2} \tag{11}$$

$$|AC| = |AA_{r1}| - |CA_{r1}| = \sqrt{l_A^2 - r^2} - r\tan\frac{\arcsin\frac{r}{l_A} - \arcsin\frac{r}{l'_A} + \theta}{2} \tag{12}$$

$$|A'C| = |A'A_{r1}| + |CA'_{r1}| = \sqrt{l_A'^2 - r^2} + r\tan\frac{\arcsin\frac{r}{l_A} - \arcsin\frac{r}{l'_A} + \theta}{2} \tag{13}$$

Similarly,

$$|AC'| = \sqrt{l_A^2 - r^2} + r\tan\frac{\arcsin\frac{r}{l'_A} + \arcsin\frac{r}{l_A} + \theta}{2} \tag{14}$$

$$|A'C'| = \sqrt{l_A'^2 - r^2} - r\tan\frac{\arcsin\frac{r}{l'_A} - \arcsin\frac{r}{l_A} + \theta}{2} \tag{15}$$

It can be found from (12), (13), (14) and (15) that

$$|AC| + |A'C| = |AC'| + |A'C'|, \tag{16}$$

which decides the shape of the formed quadrangle cannot be a trapezoid.

Parameter ranges

The construction of Bricard linkage imposes bounds for the value of each parameter. The mechanism cannot be constructed when a parameter is out of its domain of definition. Some special mechanism will be generated when the parameter has an extreme value.

For example, when $\theta = 0$, $l_A = l'_A$, and A is coincident with A'. The outline of the mechanism in the compact configuration becomes a pentagon. The locations of B and B' are no longer unique, as they can be any points on the tangent lines. The result is the construction of a Crinkle mechanism, Fig. 5.
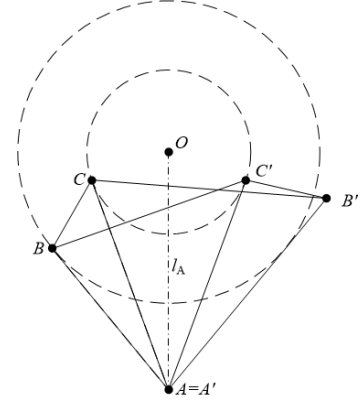

FIGURE 5. Length of the quadrangle

There are other similar cases, like when $r = R$, and B is co-incident with C. In the following, we will restrain the parameters to inside their domains of definition to avoid those special cases. The ranges are:

$$\begin{cases} 0 < r < R \\ l_A > R \\ \theta > 0 \end{cases} \tag{17}$$

In the construction of the Bricard linkage, the possible locations of B can be divided into 3 classes: B between the tangent point and A, B coinciding with A, and A between the tangent point and B.

The latter case, can be seen as exchanging A and B, A' and B' in Fig. 1. The mechanism can be equivalent to another Bricard linkage, for which B is between A and the tangent point, with different l_A, l'_A and θ. Therefore, there is another inequality condition on those four parameters. Their relationship in the limited position is shown in Fig. 6, where B and A coincide, and so do B' and A'.

To meet the constraint, R should satisfy

$$R < \frac{l_A l'_A \sin\theta}{\sqrt{l_A^2 + l_A'^2 - 2l_A l'_A \cos\theta}} \tag{18}$$
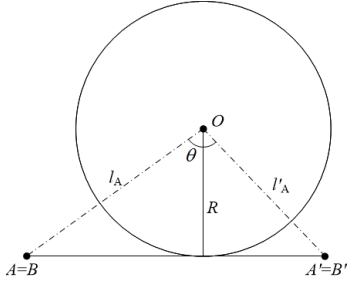
4

FIGURE 6. Limit positions of A and A'

Influence of each parameter

The shape of the quadrangle is determined by the 5 parameters of the Bricard linkage. Herein we examine the role of each variable. From (5), (6), (12), (13), (14) and (15), the angles are functions of R, l_A and l'_A, while the lengths are functions of l_A, l'_A, r and θ. To verify this result, and intuitively express the influence of each parameter, some simulations are performed in the following. There is only one variable in each simulation, the others stay constant.

Each simulation gives a series of the deployed configuration of the Bricard linkage, which illustrates the variation of the configuration (shape of the quadrangle) corresponding to the changing of the parameters. The quadrangle in red is related to the minimum value of the variable in the simulation.

To avoid discontinuity of the change of configuration, the range conditions (17) and (18) are respected in all simulations.

In the first simulation, the radius of the big circle, R, is the variable, while $r = 25$, $\theta = 90°$, $l_A = 80$ and $l'_A = 75$ are fixed. The results are shown in Fig. 7. It can be seen that the edge lengths of the quadrangle stay constant; when R increases, $\angle CAC'$ becomes bigger. The simulation result accords with (5) showing that $\angle CAC'$ covaries with R.
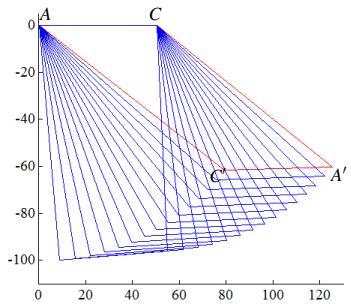

FIGURE 7. Influence of R on the two collapsed configurations

The variables in the following two simulations are θ and r, respectively, Fig. 7. Following equations (5) and (6), θ and

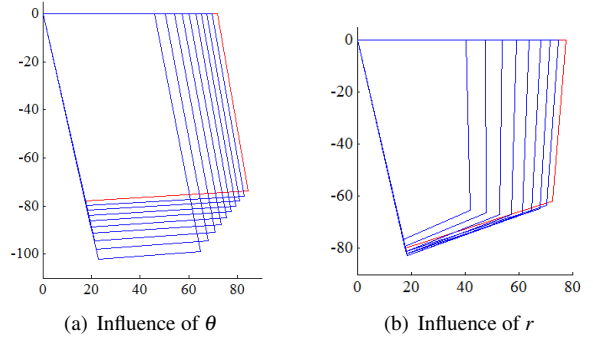r have no influence on any angle of the quadrangle; they only impact the lengths of the edges.

(a) Influence of θ (b) Influence of r

FIGURE 8. Influence of θ and r on the two collapsed configurations

Figure 9(a) and 9(b) show that l'_A does not alter the angle $\angle CAC'$ and l_A has no influence on the angle $\angle CA'C'$. However, all the edges are affected.
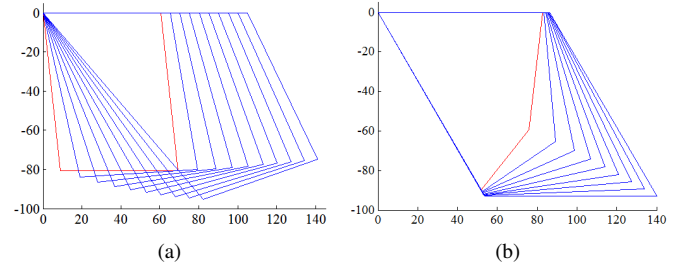

(a)   (b)

FIGURE 9. Influence of l_A and l'_A on the two collapsed configurations

Inverse calculation

In the following, the inverse calculation will be discussed, i.e., the problem of obtaining the parameter values yielding a desired planar shape.

Suppose that shape and size of the quadrangle are known, i.e., $|AC|$, $|AC'|$, $|A'C'|$, $|A'C|$, $\angle CAC' = \beta_A$, $\angle CA'C' = \beta'_A$ are all given. It can be derived that

$$\frac{R}{l_A} = \sin \frac{\beta_A}{2} \tag{19}$$

$$\frac{R}{l'_A} = \sin \frac{\beta'_A}{2} \tag{20}$$

Therefore, the ratio between l_A and l'_A is known as $\dfrac{l_A}{l'_A} = \dfrac{\sin \beta'_A/2}{\sin \beta_A/2} = n$.

From (12) and (13), we have

$$\sqrt{l_A^2 - r^2} + \sqrt{l'^2_A - r^2} = |AC| + |A'C| = l_1 \qquad (21)$$

Let $l_2 = |AC'| - |AC|$. From (14) and (12)

$$\frac{2r\sin\theta}{\cos(\arcsin\frac{r}{l_A} - \arcsin\frac{r}{l'_A}) + \cos\theta} = l_2 \qquad (22)$$

Therefore,

$$\arcsin \frac{r}{l_A} - \arcsin \frac{r}{l'_A} = \arccos \frac{2r\sin\theta - l_2\cos\theta}{l_2} \qquad (23)$$

Let $l_3 = |AC'|$, from (14) we have

$$\sqrt{l_A^2 - r^2} + r\tan \frac{\arcsin\frac{r}{l'_A} + \arcsin\frac{r}{l_A} + \theta}{2} = l_3 \qquad (24)$$

With known three lengths and two angels of the quadrangle, the values of each parameter can be obtained by solving (19)-(24).

CONNECTING TWO TYPE III BRICARD LINKAGES

Taking the type III Bricard linkage as unit, by linking each two Bricard linkage through scissor linkage or parallelogram mechanism, a network is constructed. Selection of the connecting element is decided by whether the thickness of the panel of the Bricard linkage is ignorable.

Connection via a scissor linkage

If the panel of the Bricard linkage is very thin, such as a paper model, the limitation of movement generated by the thickness of the model can be ignored. Under this condition, two Bricard linkage can be linked together by using a common hinge, as shown in Fig. 10(a). A simulated model of the assembly is shown in Fig. 10(b).

By sharing the revolute joint $A'C$ and the panel $A'B'C$, $A'BC$, two Bricard linkages are connected together, which can also be
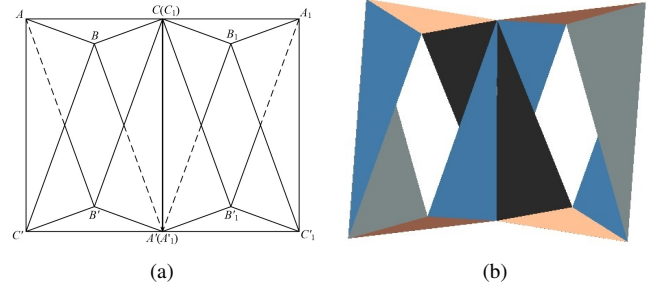

FIGURE 10. Two Bricard linkages linked by scissor linkage

seen as adding a scissor linkage in the middle of two Bricard linkages. Herein, in the assembly BCB'_1A' is one panel, $B_1CB'A'$ is another panel, and they rotate with respect to each other around $A'C$ (A'_1C_1). The vertical angles between these two panels are constantly equal. Therefore, the two Bricard linkages move synchronously.

As a type III Bricard linkage and a scissor linkage are both 1-dof, by connecting them in this way, the mobility remains the same, which also means that the number of addable Bricard linkage is unlimited.

The deployed and compact configurations of such an assembly are shown in Fig. 11. The compact configuration is the same as that of a single Bricard linkage, while the deployed configuration is doubled. The geometric shape of the deployed configuration of the assembly is totally dependent on that of the unit Bricard linkage. Furthermore, the two Bricard linkages are connected by a scissor linkage, which is a parameter-free connection, therefore, the Bricard linkages with different parameters are also able to be connected together. An example of such a case is shown in next section.
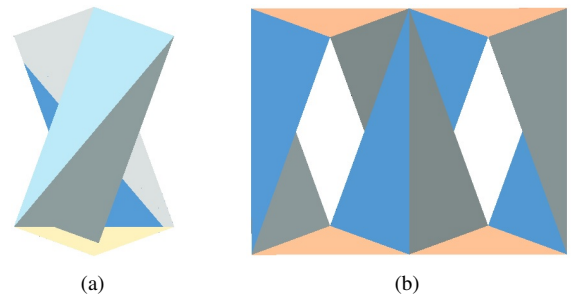

FIGURE 11. The compact and deployed configuration of the network linked with scissor linkage

6

Connection via a parallelogram mechanism

A hinged parallelogram can be used if the panel thickness cannot be ignored. The parallelogram, which also has 1-dof, plays the same role as the scissor linkage (to connect two adjacent Bricard linkages and maintain the degree of freedom) in the assembly. With the assumption that all the panels have the same thickness, parallelogram mechanisms with the same link lengths are used to construct the network. The working principle of this connection is shown in Fig. 12.
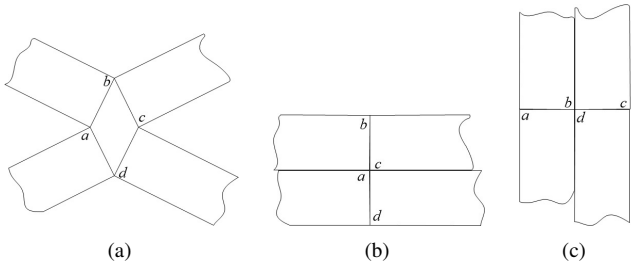

FIGURE 12.   Working principle of the parallelogram mechanism

It can be seen as a partial top view of the parallelogram mechanism connection, where joints a and c indicate the rotating axes $A'C$ and $A_1'C_1$ of the Bricard linkages. The common edges of the corresponding panels are b and d. Known from parallelogram mechanism, during the movement, $\angle bad$ is always equal to $\angle bcd$, which makes sure there is a synchronous movement between the two combined Bricard linkages. Without physical link interference, each joint can perform a half circle rotation.

In the deployed configuration, Fig. 12(b), a and c and the two side surfaces of the panel of the Bricard linkage are coincident, and the unit linkages are placed side by side. In the compact configuration, Fig. 12(c), b is coincident with d, and the units are on top of each other, which guarantees the assembly can be folded without collision, Fig. 13.

In order to avoid collision among the panels of a Bricard linkage, the shapes of the panels have been modified a little, without affecting the outline of the mechanism.
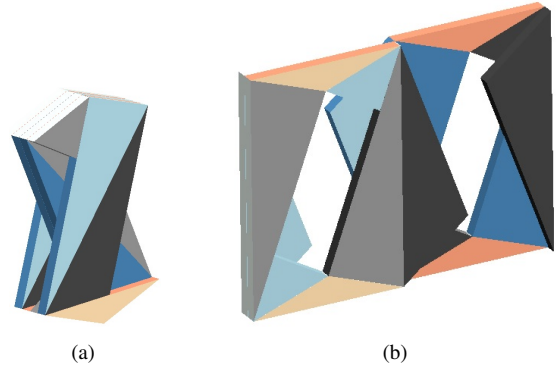

FIGURE 13.   Assembly comprised of Bricard linkages and a parallelogram mechanism

CASE STUDIES

In this section, two case studies are performed. The Bricard network deploys as a rectangle and a regular hexagon, respectively. To obtain the shapes, different Bricard parameters are adopted. Since one of the variables controls the scale of the Bricard mechanism, the radius of the small circle, r, is the same in each case.

Case I

The deployed shape of the network in this case is a rectangle. The Bricard mechanism with a rectangular outline is used as a basic unit in the network. Given $|AC| + |A'C| = |AC'| + |A'C'|$, in order to obtain a rectangular $ACA'C'$, an extra condition should be satisfied in the selected Bricard mechanism,

$$\beta_A = \beta_A' = 90°, \tag{25}$$

which yields $l_A = l_A' = \sqrt{2}R$.

Under the above conditions, θ determines the length-to-width ratio of the rectangle. When $r = 25$, $R = 50$, and $l_A = l_A' = 50\sqrt{2}$, the changing of the rectangle corresponding to different θ values is shown in Fig. 14.

A Bricard mechanism with $\theta = 20°$ is selected as the unit in the rectangular assembly. The deployment process of a paper model of the Bricard linkage network composed of 3 units is shown in Fig. 15.

In the paper model, the thickness of the panel can be ignored. Therefore, the network is constructed by using scissor elements to link the Bricard linkages. In the deployed and compact configurations, all the hinges are almost in the same plane; during the deployment process, the assembly is a spatial mechanism.
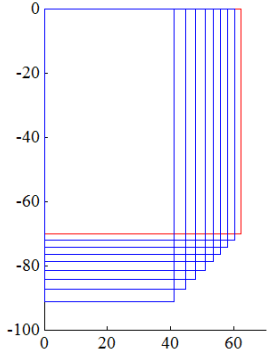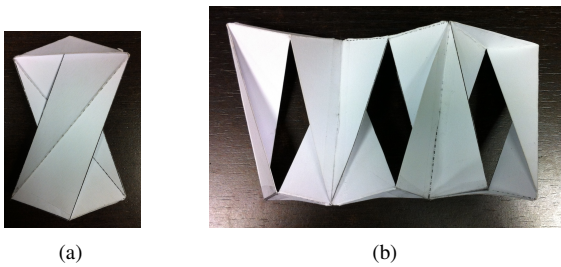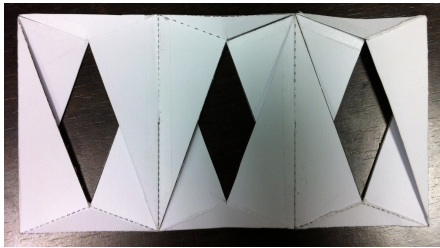
FIGURE 14. Formed rectangle corresponding to variable θ

(a)   (b)

(c)

FIGURE 15. Case study I

Case II

The network, in this case, is composed of Bricard linkages with different parameters. Outline of the assembly is a regular hexagon. The first Bricard linkage is placed at the corner of the polyhedron, the second one is on the side.

To form a hexagon, the first Bricard linkage should satisfy,

$$\beta_A = 90°, \tag{26}$$

$$\beta_C = 90° - 360°/12 = 60° \tag{27}$$

Given $r = 25$, $l_A = \sqrt{2}R = 50\sqrt{2}$, and $l'_A = 51$, $\theta = 25.41°$

is calculated from (23). Therefore, from (14), $|AC'| = 69.81$.

The outline of the second Bricard linkage is rectangle, whose long side is equal to the edge of the first quadrangle, that is $|AC'| = |A'C| = 69.81$. With given parameters $r = 25$ and $l_A = l'_A = \sqrt{2}R = 45\sqrt{2}$, it is calculated that $\theta = 48.63°$.
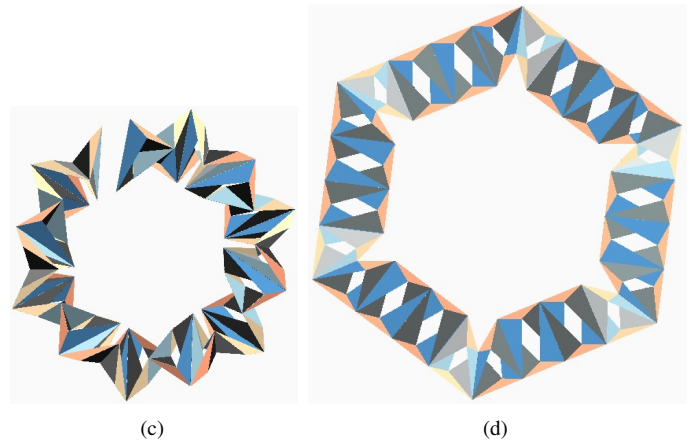
The two unit Bricard linkages are shown in Fig. 16.
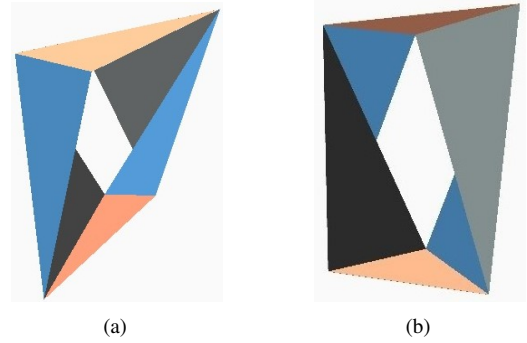
(a)   (b)

FIGURE 16. Bricard linkages in case study II

By linking 24 linkages of the above two Bricard geometries, a 3D model is built. The model is simulated and the moving process is shown in Fig. 17. Simulation of the assembly proves that a Bricard network can be constructed either using identical or different units.

(a)   (b)

(c)   (d)

FIGURE 17. Case study II

8

CONCLUSION

This paper presents a novel family of 1-dof networks of type III Bricard linkages. Each such deployable mechanism can cover an arbitrarily large surface with a specific outline when deployed, and can be folded compactly into a stack of much smaller planar shapes. The type III Bricard mechanism is described by five geometric parameters, the relationship among the parameters and the outline of the deployed configuration of the Bricard linkage is discussed. Parameter range constraints for constructing the mechanism are derived. Inverse calculation to obtain the parameter values yielding a desired planar shape is performed. The Bricard network can be built in two ways, linked by scissor linkages, when thickness of the panels can be ignored, or by parallelograms if the material is thick.

Two case studies have been performed, which present the procedure of obtaining a deployed rectangle and regular hexagon, respectively. It is also illustrated that Bricard linkages with different parameters can be linked together. Simulations of the obtained assembly validate the proposed analysis and design methods.

This paper focuses on the Bricard linkage built by the triangular panels in Fig. 1. The outline of the linkage and the network is formed by the vertices of the Bricard linkage. It is known that the structural design of a mechanism may vary its geometric shape dramatically. Some possible such variations will be reported in future work.

ACKNOWLEDGEMENT

REFERENCES

[1] F. Escrig, J. P. Valcarcel, and J. Sanchez. Deployable cover on a swimming pool in Seville. *Bulletin of the International Association for Shell and Spatial Structures*, 37(1):39–70, 1996.

[2] J. S. Zhao, J. Y. Wang, F. L. Chu, Z. J. Feng, and J. S. Dai. Mechanism synthesis of a foldable stair. *Journal of Mechanisms and Robotics*, 4(1):014502, 2012.

[3] G. Durand, M. Sauvage, A. Bonnet, L. Rodriguez, et al. Talc: a new deployable concept for a 20-m far-infrared space telescope. In *SPIE Astronomical Telescopes+ Instrumentation*, pages 91431A–91431A. International Society for Optics and Photonics, 2014.

[4] C. Hoberman. *Radial expansion/retraction truss structures*, June 18 1991. US Patent 5,024,031.

[5] F. Maden, K. Korkmaz, and Y. Akgün. A review of planar scissor structural mechanisms: geometric principles and design methods. *Architectural Science Review*, 54(3):246–257, 2011.

[6] Y. Chen. *Design of structural mechanisms*. PhD thesis, University of Oxford, 2003.

[7] S. Y. Liu and Y. Chen. Myard linkage and its mobile assemblies. *Mechanism and Machine Theory*, 44(10):1950–1963, 2009.

[8] X. Z. Qi, Z. Q. Deng, B. Li, R. Q. Liu, and H. W. Guo. Design and optimization of large deployable mechanism constructed by Myard linkages. *CEAS Space Journal*, 5(3-4):147–155, 2013.

[9] R. Bricard. Mémoire sur la théorie de l'octaèdre articulé. *Journal de Mathématiques pures et appliquées*, pages 113–148, 1897.

[10] A. V. Bushmelev and I. Kh. Sabitov. Configuration spaces of Bricard octahedra. *Journal of Mathematical Sciences*, 53(5):487–491, 1991.

[11] J. E. Baker. On the skew network corresponding to Bricard's doubly collapsible octahedron. *Proceedings of the Institution of Mechanical Engineers, Part C: Journal of Mechanical Engineering Science*, 223(5):1213–1221, 2009.

[12] M. Goldberg. Linkages polyhedral. *National Mathematics Magazine*, 16(7):323–332, 1942.